Numerical Integration of the Navier-Stokes Equations for a Disk Rotating in a Housing*

A. F. Borghesani, L. Bruschi
Dipartimento di Fisica dell'Università di Padova, Italy
and Gruppo Nazionale Struttura della Materia, Padova, Italy

Z. Naturforsch. **40 a**, 789–799 (1985); received March 25, 1985

The Navier-Stokes equations for the fluid motion induced by a disk rotating inside a cylindrical cavity have been integrated for several values of the boundary layer thickness δ. The equivalence of such a device to a rotating disk immersed in an infinite medium has been shown in the limit as $\delta \to 0$.

From that solution and taking into account edge effect corrections an equation for the viscous torque acting on the disk has been derived, which depends only on δ. Moreover, these results justify the use of a rotating disk to perform accurate viscosity measurements.

PACS numbers: 0270, 0340G, 4715C

§ 1. Introduction

A rotating disk viscometer has recently been devised [1, 2] to perform accurate viscosity measurements in the critical region of fluids. This viscometer (Fig. 1) consists of a thin copper disk supported by a pivot inside a cylindrical cavity filled with the fluid to be investigated. The disk is set into rotation by the interaction between the eddy currents induced in its body by two small opposing electromagnets.

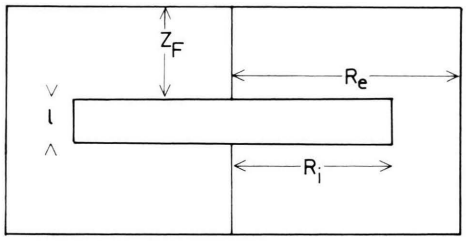

Fig. 1. Schematic drawing of the rotating disk viscometer (not to scale). The rotating disk is a cylinder of radius R_i and height l ($l \ll R_e$) enclosed into a cylindrical cavity, which has a radius R_e and a height $(2z_F + l)$. Each disk face is separated from the wall of the cavity by a distance z_F known as the separation gap. In the actual disk $(R_e - R_i) \simeq 4z_F$ and $z_F \simeq 4(l/2)$.

* Work supported by Consiglio Nazionale delle Ricerche and Ministero Pubblica Istruzione, Rome, Italy.

Reprint requests to Dr. A. F. Borghesani, Dipartimento di Fisica, Univ. Padova, Via F. Marzolo, 8, 35131 Padova (I).

In the steady state the torque balance requires:

$$\tau_e + \tau_\eta = 0, \tag{1.1}$$

where τ_e is the effective driving torque on the disk including the net driving torque due to the eddy currents and the retarding torque due to the friction of the disk pivot on its bearings. τ_η is the retarding torque due to the fluid-disk interaction and depends on the angular velocity of the disk, ω, and on the viscosity and density of the fluid, η and ϱ. From measurements of ω, ϱ and τ_e, the viscosity of the fluid can be computed through the dependence of τ_η on ω and ϱ.

Unfortunately, there is not yet a general hydrodynamic solution for τ_η in the laminar regime [3], but it is known in two limiting cases:

$$\tau_\eta \propto \eta\,\omega/z_F \quad \text{for} \quad \delta \gg z_F, \tag{1.2}$$

$$\tau_\eta \propto \eta\,\omega/\delta \quad \text{for} \quad \delta \ll z_F, \tag{1.3}$$

where $\delta = (\nu/\omega)^{1/2}$ is the boundary layer thickness, $\nu = \eta/\varrho$ is the kinematic viscosity of the fluid and z_F is the gap separating the disk and the housing walls (Figure 1).

The behaviour of τ_η between these two extreme cases is not known, and it is therefore necessary to find an analytical empirical expression for it by performing measurements with a fluid of known density and viscosity. It has been assumed [1, 2] that the following relationship holds:

$$\tau_\eta = -\mu\,\eta\,\omega\,f^{-1}(\delta), \tag{1.4}$$

0340-4811 / 85 / 0800-0789 $ 01.30/0. – Please order a reprint rather than making your own copy.

where μ is a constant and $f(\delta)$ is a well-suited function of the boundary layer thickness. Now, the question arises whether (1.4) is universally valid for all fluids. The answer to this question becomes affirmative if one shows that the viscous torque determined by solving the Navier-Stokes (NS) equations for the disk rotating in a housing can be expressed by (1.4) and that its δ-dependence has the same analytical form as that determined by measurements in a particular fluid. That is precisely what has been done as it will be explained in the next sections.

Even if the final goal of the present paper is to give a quantitative estimation of the torque acting on the disk and to compare this with the experiment, nevertheless the main body of the paper is "a fortiori" concerned with the NS equations and with the problem of their integration.

The physical and mathematical problem of the equations of the fluid motion in the case of a disk of infinite radius rotating between two parallel infinite planes is set out in § 2. In § 3 the relationship between the solution of the Navier-Stokes equations and the torque τ_η acting on the infinite disk is presented. Edge effect corrections are then introduced to give an equation for τ_η for an actual disk. The numerical integration procedure for the NS equations and the numerical results in terms of the fluid velocity components are described and presented in § 4 and § 5, respectively. In § 6 it is shown that the differential equations for the disk in the housing in the limit as $\delta \to 0$ tend to those for the disk immersed in an infinite medium. A numerical check of the procedure is then performed. In § 7 the numerical results for τ_η are compared with the experimental data.

Finally, the conclusions are drawn in § 8.

§ 2. The Navier-Stokes Equations for a Steady-State Rotating Disk in a Housing

We are searching for steady-state solutions of the Navier-Stokes equations in case of cylindrical symmetry around the disk axis. Let us refer to a system of cylindrical coordinated with the z-axis parallel to the disk-axis and let $v_r(r, z)$, $v_\varphi(r, z)$ and $v_z(r, z)$, respectively, be the radial, tangential and axial components of the fluid velocity and P the pressure.

The Navier-Stokes and the continuity equations are then [4]

$$v_r \frac{\partial v_r}{\partial r} + v_z \frac{\partial v_r}{\partial z} - \frac{v_\varphi^2}{r} = -\frac{1}{\varrho}\frac{\partial P}{\partial r} + \nu\left(\frac{\partial^2 v_r}{\partial r^2} + \frac{\partial^2 v_r}{\partial z^2} + \frac{1}{r}\frac{\partial v_r}{\partial r} - \frac{v_r}{r^2}\right), \tag{2.1}$$

$$v_r \frac{\partial v_\varphi}{\partial r} + v_z \frac{\partial v_\varphi}{\partial z} + \frac{v_r v_\varphi}{r} = \nu\left(\frac{\partial^2 v_\varphi}{\partial r^2} + \frac{\partial^2 v_\varphi}{\partial z^2} + \frac{1}{r}\frac{\partial v_\varphi}{\partial r} - \frac{v_\varphi}{r^2}\right), \tag{2.2}$$

$$v_r \frac{\partial v_z}{\partial r} + v_z \frac{\partial v_z}{\partial z} = -\frac{1}{\varrho}\frac{\partial P}{\partial z} + \nu\left(\frac{\partial^2 v_z}{\partial r^2} + \frac{\partial^2 v_z}{\partial z^2} + \frac{1}{r}\frac{\partial v_z}{\partial r}\right), \tag{2.3}$$

$$\frac{1}{r}\frac{\partial}{\partial r}(r v_r) + \frac{\partial v_z}{\partial z} = 0, \tag{2.4}$$

with the boundary conditions

$$v_r(r, 0) = 0, \tag{2.5}$$

$$v_\varphi(r, 0) = \omega r, \tag{2.6}$$

$$v_z(r, 0) = 0, \tag{2.7}$$

$$v_r(r, z_F) = 0, \tag{2.8}$$

$$v_\varphi(r, z_F) = 0, \tag{2.9}$$

$$v_z(r, z_F) = 0. \tag{2.10}$$

It must be emphasized that we are dealing now with a disk of infinite radius, and that a similarity solution is assumed to get rid of the partial derivatives in the previous equations. For the moment any edge effects for a disk of finite radius are ignored. We will account for them later on. Moreover, when the flow in the boundary layer is radially inwards, as it will be seen in our case, the question of the range of validity of the similarity solution has still to be settled [5]. At present we will not worry about it.

Following v. Kármán [6] we therefore assume

$$v_r = \omega r F(z_1), \tag{2.11}$$

$$v_\varphi = \omega r G(z_1), \tag{2.12}$$

$$v_z = (\nu\omega)^{1/2} H(z_1), \tag{2.13}$$

$$z_1 = z/\delta. \tag{2.14}$$

The z-axis has the direction of $\vec{\omega}$ and the planes $z=0$ and $z=\pm z_F$ correspond to the rotating disk and to the housing walls, respectively.

It can be recognized that the axial velocity (2.13) has no radial dependence, i.e., it is uniform over planes parallel to the disk surface. This is a good approximation for an infinite disk, but surely not for a finite one, because in that case the streamlines must be closed. However, this approximation, $v_z = v_z(z_1)$, can still be accepted for a finite disk if $z_F \ll R_i$, where R_i is the disk radius, and if the lateral gap $R_e - R_i$ is much larger than δ.

In the case of a disk in an infinite fluid, pressure is further assumed to be a function only of z_1 [6–8]. In our case, however, we are forced allowing P to be a function of r and z_1, and not in a separable way. This can be understood by the following reasoning [9].

By virtue of (2.13) and (2.11) the continuity equation (2.4) can be immediately integrated to give

$$2F(z_1) + H'(z_1) = 0, \tag{2.15}$$

where the prime indicates differentiation with respect to z_1. Then, (2.3) is easily integrated yielding

$$P(r, z_1) = \varrho \nu \omega \left(H'(z_1) - \tfrac{1}{2} H^2(z_1)\right) + \Pi(r), \tag{2.16}$$

where $\Pi(r)$ is a constant of the integration with respect to z_1. By substituting (2.16) and (2.15) into (2.1) we get

$$\frac{1}{\varrho \omega^2 r} \frac{\partial \Pi(r)}{\partial r} = (F'' - F^2 - HF' + G^2) \equiv \gamma_1, \tag{2.17}$$

where γ_1 is a constant, independent of both r and z_1, because the l.h.s. of (2.17) is a function only of r, while the r.h.s. is only a function of z_1.

By integrating (2.17) with respect to r and substituting into (2.16) we get

$$P(r, z_1) = \varrho \nu \omega \left(H'(z_1) - \tfrac{1}{2} H^2(z_1)\right) + \tfrac{1}{2} \varrho \gamma_1 \omega^2 r^2 + P_0, \tag{2.18}$$

where it is evident that $P(r, z_1)$ cannot be expressed by a product of a function of r times a function of z_1.

Now the NS equations (2.1) and (2.2) and the continuity equation (2.4) become

$$F'' = \gamma_1 + F^2 - G^2 + HF', \tag{2.19}$$

$$G'' = HG' + 2FG, \tag{2.20}$$

$$H' = -2F \tag{2.21}$$

with the boundary conditions

$$F(0) = H(0) = F(b) = G(b) = H(b) = 0,$$
$$G(0) = 1 \quad (b = z_F/\delta). \tag{2.22}$$

Equation (2.18) will immediately give the pressure once (2.19–21) are integrated. However, (2.19) cannot be integrated because the constant γ_1 is known only in the case of the disk immersed in an infinite fluid. In this case, F and G must vanish with all their derivatives as $z_1 \to \infty$, so that $\gamma_1 = 0$ from (2.17). This also means that $\Pi(r) \equiv P_0$ from (2.17) and that $(P - P_0)$ is only a function of z_1 from (2.18).

On the contrary, in our case, at $z_1 = b$ only F, G and H vanish, but not necessarily their derivatives, too. Therefore, $\gamma_1 \neq 0$. But as $\delta \to 0$, $b \to \infty$ and the equations for the disk in the housing must converge to those of the free disk. On these grounds, we expect that γ_1 depends on δ, but still in an unknown way.

To overcome this difficulty, (2.19) is differentiated with respect to z_1 and the following set of non linear differential equations is obtained:

$$F''' = HF'' - 2GG', \tag{2.23}$$

$$G'' = HG' + 2FG, \tag{2.24}$$

$$H' = -2F \tag{2.25}$$

with boundary conditions (2.22).

The system (2.23–25) must be integrated for different values of δ (or, conversely, for different b) and its equivalence to the system for a disk immersed in an infinte fluid must also be demonstrated by showing that

$$\lim_{\delta \to 0} \gamma_1 = \lim_{\delta \to 0} (F'' - F^2 + G^2 - HF') = 0.$$

§ 3. Relationship between the Exact Solutions of the NS Equations and the Viscous Torque on the Disk in the Housing

By neglecting edge effects, the torque acted by the fluid on both sides of the disk of radius R_i is given by [4]

$$\tau_\eta^{(d)} = \pi R_i^4 \eta \omega \frac{G'(0)}{\delta} \equiv -\frac{\pi R_i^4}{z_F} \eta \omega g^{-1}(\delta), \tag{3.1}$$

where $G'(0) \equiv \left[\dfrac{dG(z_1)}{dz_1}\right]_{z_1=0}$ and $G(z_1)$ is the z_1-dependent part of the tangential component of the fluid velocity.

However, edge effects on the velocity field due to the boundary must be taken into account.

Actual disks are not indefinitely thin. The housing walls tangentially decelerate the fluid inducing a radial gradient of the tangential velocity. The fluid in the housing is also sheared by the lateral cylindrical surface of the disk. This results in a tangential stress acting on the disks lateral surface [10]. As a consequence of this, the tangential velocity $v_\varphi (r \geq R_i, z = 0)$ cannot depend linearly on the disk radius. It must be replaced by the more general expression

$$v_\varphi (r, z = 0) = \omega (r + h (r)), \quad (r \geq R_i), \tag{3.2}$$

where $h (r)$ is a well-suited function describing the deviation of the tangential velocity field from the linear law (2.12). The function $h (r)$ must furthermore be well-behaved so as to satisfy the requirements

$$h (r) = 0 \quad \text{for} \quad r \leq R_i, \tag{3.3}$$

$$h (R_e) = - R_e. \tag{3.4}$$

This radial dependence of the tangential velocity produces a retarding torque expressed by

$$\tau_\eta^{(g)} = (2 \pi l R_i^3) \eta \omega \left[\frac{\partial}{\partial r} \frac{h (r)}{r} \right]_{r = R_i^+} \equiv - \pi R_i^4 k_1 \eta \omega, \tag{3.5}$$

where $k_1 = - \dfrac{2 l}{R_i} \left[\dfrac{\partial}{\partial r} \dfrac{h (r)}{r} \right]_{r = R_i^+}$.

Summing up all these contributions, the total torque on the disk is

$$\tau_\eta = \tau_\eta^{(d)} + \tau_\eta^{(g)} = \frac{- \pi R_i^4}{z_F} (g^{-1} (\delta) + k) \eta \omega, \tag{3.6}$$

where $k = k_1 z_F$.

It must now be pointed out that in an actual experiment k_1 is not known because there is no information about the analytical from of $h (r)$. Therefore the value of k_1 must be adjusted to fit experimental data, even if an exact matching cannot be expected, because of smaller edge effects neglected in equation (3.6).

§ 4. The Procedure of Numerical Integration of (2.23 – 25) with Boundary Conditions (2.22)

The system of differential equations (2.23–25) can be put, as usually, in a form to make numerical integration easier by letting $F = y_1$, $G = y_4$, $H = y_6$, $F' = y_2$, $F'' = y_3$ and $G' = y_5$. One thus obtains a set of six first-order nonlinear differential equations. This set presents several difficulties to its solution, mainly because it is non-linear and there are only the 3 boundary conditions for $z_1 = 0$, $y_1 (0) = y_6 (0) = 0$ and $y_4 (0) = 1$, (the other 3 boundary conditions being $y_1 (b) = y_4 (b) = y_6 (b) = 0$).

For these reasons finite differences integration schemes have been disregarded, and the following procedure has been adopted [11].

The set of six non-linear differential equations has been linearized thus giving

$$\dot{y}_1 = y_2, \tag{4.1}$$

$$\dot{y}_2 = y_3, \tag{4.2}$$

$$\begin{aligned} \dot{y}_3 = {} & y_3^{(0)} y_6^{(0)} - 2 y_4^{(0)} y_5^{(0)} + y_6^{(0)} (y_3 - y_3^{(0)}) \\ & + y_3^{(0)} (y_6 - y_6^{(0)}) \\ & - 2 \{ y_4^{(0)} (y_5 - y_5^{(0)}) + y_5^{(0)} (y_4 - y_4^{(0)}) \}, \end{aligned} \tag{4.3}$$

$$\dot{y}_4 = y_5, \tag{4.4}$$

$$\begin{aligned} \dot{y}_5 = {} & y_5^{(0)} y_6^{(0)} + 2 y_1^{(0)} y_4^{(0)} + y_6^{(0)} (y_5 - y_5^{(0)}) \\ & + y_5^{(0)} (y_6 - y_6^{(0)}) \\ & + 2 \{ y_4^{(0)} (y_1 - y_1^{(0)}) + y_1^{(0)} (y_4 - y_4^{(0)}), \end{aligned} \tag{4.5}$$

$$\dot{y}_6 = - 2 y_1, \tag{4.6}$$

where $y_j^{(0)}$ $(j = 1, 6)$ are suitable zeroth-order approximations of y_j. To integrate (4.1–6) a third-order Runge-Kutta method has been chosen, because we expected F, G, and H to be smooth functions of z_1 (as "a posteriori" verified) and because at each iteration of the integration cycle of (4.1–6) it is necessary to know the values the functions had at the previous iteration.

To obviate to the absence of 3 further conditions at $z_1 = 0$, the linearized system with its boundary conditions has been integrated four times, imposing on $y_2 (0)$, $y_5 (0)$, and $y_3 (0)$ different arbitrary values each time.

Let $y_{jn}^{(1)}$ be the first-order approximations of y_j at the end of the first iteration of the four simultaneous integrations, where $n = 1, 4$ refers to the n-th integration.

The general solutions of our problem are linear combinations of the solutions of the four different integrations.

Let us therefore construct the following linear combinations:

$$y_j^{(1)} = \sum_{n=1}^{4} c_n y_{jn}^{(1)}, \tag{4.7}$$

$$y_j^{(0)} = \sum_{n=1}^{4} c_n y_{jn}^{(0)}. \tag{4.8}$$

The coefficients c_n are obtained by imposing 3 boundary conditions on y_1, y_4 and y_6 at $z_1 = b$ and one boundary condition on y_4 at $z_1 = 0$.

A set of linear algebraic equations results, which in matrix notation yields:

$$\hat{D}\,\hat{C} = \hat{Y}_c. \tag{4.9}$$

Here

$$\hat{C} = \begin{pmatrix} c_1 \\ c_2 \\ c_3 \\ c_4 \end{pmatrix} \tag{4.10}$$

is a column vector containing the coefficients c_n,

$$\hat{Y}_c = \begin{pmatrix} y_4(0) \\ y_1(b) \\ y_4(b) \\ y_6(b) \end{pmatrix} \tag{4.11}$$

is the column vector containing the known terms and

$$\hat{D} = \begin{pmatrix} 1 & 1 & 1 & 1 \\ y_{11}^{(1)}(b) & y_{12}^{(1)}(b) & y_{13}^{(1)}(b) & y_{14}^{(1)}(b) \\ y_{41}^{(1)}(b) & y_{42}^{(1)}(b) & y_{43}^{(1)}(b) & y_{44}^{(1)}(b) \\ y_{61}^{(1)}(b) & y_{62}^{(1)}(b) & y_{63}^{(1)}(b) & y_{64}^{(1)}(b) \end{pmatrix} \tag{4.12}$$

contains the values at the boundaries of $y_1 y_4 y_6$ in the four different simultaneous integrations.

Since system (4.1−6) is a linearized one, we must require that its solutions $y_j^{(1)}$ (4.7) converge to the true solutions of the original system of non-linear differential equations.

Let therefore ε be an arbitrary small positive number (in our case we have chosen $\varepsilon = 10^{-7}$) and consider the inequality

$$\max_{\substack{1 \le j \le 6 \\ 0 \le z_1 \le b}} \{ | y_j^{(1)}(z_1) - y_j^{(0)}(z_1) | \} \le \varepsilon. \tag{4.13}$$

Should (4.13) not be satisfied by (4.7) and (4.8), then the $y_{jn}^{(1)}$ are taken as new zeroth-order approximations of the true y_{jn}. The complete cycle of 4 simultaneous integrations is then repeated, thus determining the next approximations, until the convergence criterion (4.13) is satisfied. If m is the number of iterations required to satisfy (4.13), the required solutions are given by

$$y_j = \sum_{n=1}^{4} c_n y_{jn}^{(m)}, \tag{4.14}$$

where $y_{jn}^{(m)}$ are the m-th-order approximations of the true y_{jn}. Unfortunately, this procedure is not apt to ensure the stability of the solutions to within the desired degree of accuracy, $\varepsilon = 10^{-7}$.

In fact, if we drastically change the arbitrary values of $y_{2n}(0)$, $y_{5n}(0)$, $y_{3n}(0)$ $(n = 1, 4)$ we get a change of some parts per thousand in the solutions. This is a very severe drawback, for we are particularly interested in $y_5(0)$. We therefore forced the solutions of one of the four integrations (e.g. the first) to converge to the true solutions.

The procedure to obtain this goal is very simple.

Once the convergence criterion (4.13) has been satisfied, we look for the quantities

$$\varepsilon_1 = | y_{21}^{(m)}(0) - y_2(0) |, \tag{4.15}$$

$$\varepsilon_2 = | y_{31}^{(m)}(0) - y_3(0) |, \tag{4.16}$$

$$\varepsilon_3 = | y_{51}^{(m)}(0) - y_5(0) |. \tag{4.17}$$

If ε_1, ε_2 and ε_3 are not simultaneously smaller than ε, then $y_2(0)$, $y_3(0)$, and $y_5(0)$, computed through (4.14), are taken as arbitrary conditions on $y_{21}(0)$, $y_{31}(0)$, and $y_{51}(0)$. The arbitrary conditions on $y_{2k}(0)$, $y_{3k}(0)$, and $y_{5k}(0)$ $(k = 2, 4)$ are, however, unaltered. The whole preceding procedure is then repeated from the beginning by letting $y_{j_1}^{(0)} = y_j$ and $y_{jk}^{(0)} = y_{jk}^{(m)}$ $(k = 2, 4)$ until $\varepsilon_l \le \varepsilon$ for each $l = 1, 3$.

In such a way $c_1 \approx 1$, $c_2 \approx 0$, $c_3 \approx 0$, and $c_4 \approx 0$ at the end of the calculations. The stability of the solutions with respect to the arbitrary conditions in the origin is now satisfactorily high, showing absolute differences $\le 10^{-6}$.

Finally, a comment on the choice of the zeroth-order functions $y_{jn}^{(0)}$: For small b (large δ) v_r and v_z are about zero [10, 12] and $G(z)$ is a straight line to a good approximation. So, for small b, $y_{4n}^{(0)}(z_1) = 1 - z_1/b$ and $y_{jn}^{(0)}(z_1) = y_{jn}(0)$ $(n = 1, 4, j \neq 4)$. For large b (small δ) this choice is not so good as before, and the algorithm diverges. Therefore, the solutions for a particular b, say b_0, are taken as zeroth-order approximations of the solutions for $b > b_0$ and so on. In such a way the algorithm does never diverge.

§ 5. Numerical Results for the Velocity Components F, G, and H

In Figs. 2, 3, 4 the results of the numerical integration of (2.23–25) are reported in the three interesting cases

a) $\delta \gg z_F$, b) $\delta = z_F$, c) $\delta \ll z_F$.

In Fig. 2 the results of the numerical integration as functions of z_1 for $\delta = 10\, z_F$ ($b = 0.1$). Function G is a straight line joining point (0, 1) with point (b, 0) and having a slope of -10. $F(z_1)$ and $H(z_1)$ are both practically zero ($\max_{0 \le z_1 \le b} |F(z_1)| < 9 \times 10^{-5}$ and $\max_{0 \le z_1 \le b} |H(z_1)| < 5 \times 10^{-6}$). The resulting flow is therefore of the Couette-type: the fluid only rotates around the symmetry axis with neither radial nor axial velocity components. The tangential velocity is then given by

$$v_\varphi = \omega\, r\,(1 - z_1/b). \tag{5.1}$$

The value of $G'(0)$ is $-10 = -1/b$. Recalling that $b = z_F/\delta$ we find $G'(0) = -\delta/z_F$ or

$$-\frac{G'(0)}{\delta} = \frac{1}{z_F} = \text{const} \tag{5.2}$$

or $g(\delta) = 1$.

Substituting (5.2) into (3.6) we have

$$\tau_\eta \propto \eta\, \omega / z_F \tag{5.3}$$

which is precisely the result expressed by (1.2).

The case $\delta = z_F$ ($b = 1$) is depicted in Figure 3. $G(z_1)$ is still almost a straight line. The fluid has acquired small, but non-zero components of velocity in the radial and axial directions ($\max_{0 \le z_1 \le b} |F(z_1)| \simeq 8.5 \times 10^{-3}$ and $\max_{0 \le z_1 \le b} |H(z_1)| \simeq 5.2 \times 10^{-3}$).

$G'(0) \simeq -1.0043$ does not anymore depend upon b (or δ) in a simple manner. It results $-G'(0) > 1/b$

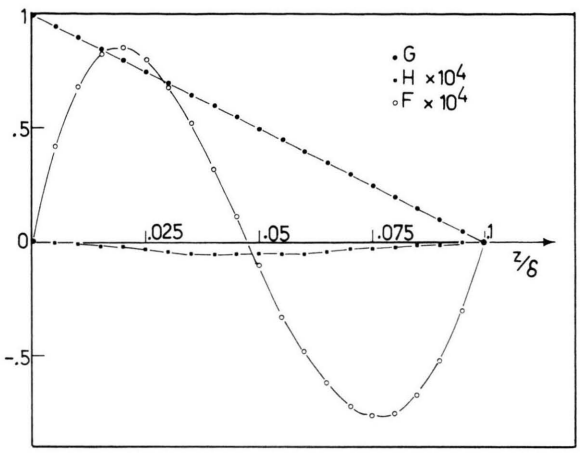

Fig. 2. z_1-dependent parts of the fluid velocity components for $z_F/\delta = 0.1$. Open circles $F(z_1)$, closed circles $G(z_1)$ and closed squares $H(z_1)$. $G(z_1)$ is a straight line and F and H (very enlarged in the drawing) are nearly zero and fairly symmetric with respect to the gap center $z_1 = 0.05$.

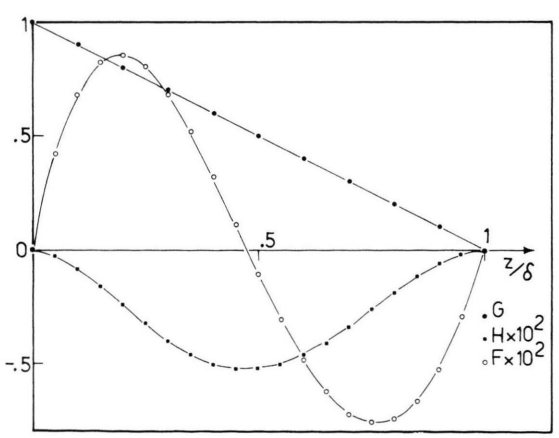

Fig. 3. F, G, and H as functions of $z_1 = z/\delta$ for $z_F/\delta = 1$. (Symbols as in the previous figure.) In this case the boundary layer thickness equals the separation gap. G is a straight line to a good approximation. F and H are still small. The asymmetry of F and H with respect to $z_1 = 0.5$ is not yet very pronounced.

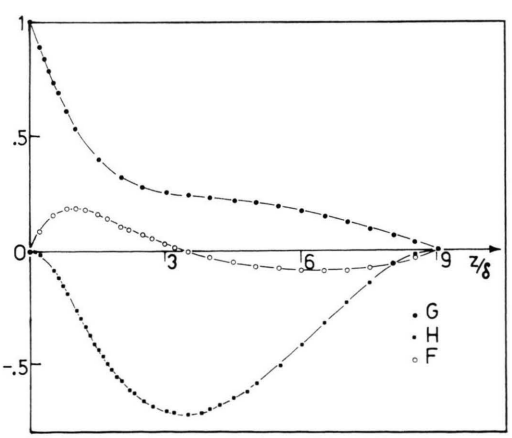

Fig. 4. F, G, and H as functions of z_1 for $z_F/\delta = 9$. (Symbols as in the previous figure.) $G(z_1)$ cannot be approximated by a straight line but changes concavity. F and H are now macroscopically different from zero. Their asymmetry with respect to $z_1 = 4.5$ is selfevident.

$= \delta/z_F$ and thus $-\dfrac{G'(0)}{\delta} > z_F^{-1}$. This means $|\tau_\eta| > \eta\omega/z_F$ as expected from (1.2) and (1.3) as $\delta \gtrsim z_F$.

Finally, the case $\delta = \frac{1}{9} z_F$ ($b = 9$) is depicted in Figure 4. The fluid now possesses large radial and axial velocity components. F is such that $\int_0^b F(z_1)\,dz_1 = 0$ so as to satisfy the continuity equation. The axial velocity component, described by $H(z_1)$, is correctly directed towards the disk to compensate the fluid displacement due to the action of the disk as a centrifugal fan.

The function $G(z_1)$ does not resemble anymore a straight line. Particularly, its second derivative does indeed change sign in [0, b] and $G(1) \simeq 0.53$. This means that δ is the distance from the disk over which the tangential velocity of the fluid is reduced to about half the disk velocity. The largest change in $G(z_1)$ is restricted to the range $0 \leq z_1 < 2$. Then $G(z_1)$ decreases much more slowly. At about half the way between disk and housing wall $G'(4) \simeq -0.020$, about 1/30 of $G'(0) \simeq -0.56$. In the neighbourhood of $z_1 = 4.0$, $G''(z_1) \simeq 0$ and G changes concavity. For $z_1 > 4.0$ $|G'(z_1)|$ again increases up to $G'(9) \simeq -0.063$.

This increase of $|G'(z_1)|$ indicates that a kind of a boundary layer is also formed at the housing wall, even if the tangential velocity variation in this layer is not as sharp as in the boundary layer at the disk. In this secondary boundary layer the radial velocity component is negative showing that in this layer there is an inwards flow compensating the outwards flow in the boundary layer at the rotating disk.

In the region where $|G'|$ is minimum or nearly minimum the radial velocity is nearly zero, because $F \approx 0$.

Furthermore, F, G, and H do not have symmetry properties with respect to the plane $z_1 = 4.5 = b/2$.

All these results are in qualitative agreement with previous experimental observations [12].

§ 6. Comparison between the Sets of Differential Equations for a Disk in a Housing and for a Disk in an Infinite Fluid. Their Equivalence in the Limit as $\delta \to 0$.

The set of differential equations for the disk in a housing is given by Eqs. (2.19–21) with boundary conditions (2.22). For a disk in an infinite fluid [6], F, G, and H satisfy the set of differential equations

$$F'' = HF' + F^2 - G^2, \tag{6.1}$$

$$G'' = HG' + 2FG, \tag{6.2}$$

$$H' = -2F \tag{6.3}$$

which only needs 5 boundary conditions: $F(0) = H(0) = F(\infty) = G(\infty) = 0$, $G(0) = 1$.

It is a natural choice to give up the condition on $H(\infty)$ in going from (2.19–21) to (6.1–3), because it is necessary not to fix the value of H at infinity in order to satisfy the continuity equation when $\int_0^\infty F(z_1)\,dz_1 \neq 0$.

System (2.19–21) must however converge to system (6.1–3) as the gap between disk and housing walls for a given δ indefinitely increases. However, this is equivalent to an indefinite decrease of δ at fixed gap separation. This is also obvious from a physical argument. In fact, as $\delta \to 0$ the largest velocity gradients are restricted to a layer very thin with respect to the gap, and the disk has no way at all to perceive the presence of a wall at such a large distance. It is easy to see that system (2.19–21) reduces to system (6.1–3) as $\delta \to 0$ if $\lim_{\delta \to 0} \gamma_1(\delta) = 0$.

The δ-dependence of $\gamma_1 = F'' - F^2 + G^2 - HF'$ is shown in Figure 5. It results to be a smooth function of the boundary layer thickness and goes to zero as $\delta \to 0$. It therefore behaves correctly at small δ, thus

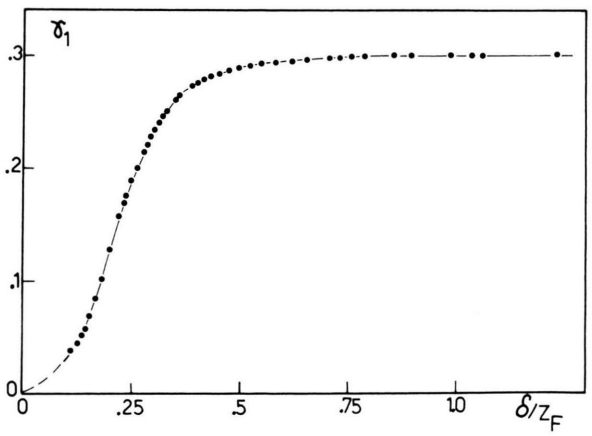

Fig. 5. Values of $\gamma_1 \equiv F'' - (F^2 - G^2 + HF')$ as functions of the boundary layer thickness scaled by the gap separation (Dashes indicate graphical extrapolation). For large δ/z_F, γ_1 saturates to a constant value of about 0.3; for small δ/z_F, it tends to zero.

showing the equivalence of system (2.19–21) to system (6.1–3). As δ becomes very large, γ_1 saturates to a constant value, $\gamma_1 \simeq 0.3$. This means that for large δ (2.18) yields

$$P(r, z_1) \simeq P_0 + \varrho \nu \omega (H'(z_1) - \tfrac{1}{2} H^2(z_1)) + 0.15\, \varrho\, \omega^2 r^2. \quad (6.7)$$

(This formula does not hold of course for a disk of infinite radius!) On the contrary, in the limit as $\delta \to 0$, (2.18) reduces to

$$P(r, z_1) = P_0 + \varrho \nu \omega (H'(z_1) - \tfrac{1}{2} H'(z_1)). \quad (6.8)$$

In this case the pressure does not depend upon r and is a function only of z_1 as expected [3, 4, 6].

Finally, to check our integration procedure, system (6.1–3) has been integrated for $\gamma_1 = 0$ with boundary conditions $F(0) = H(0) = F(b) = G(b) = 0$, $G(0) = 1$ for several upper integration limits up to $b = 8$. The results for $b = 8$ are compared to those of v. Kármán-Cochran [3, 6] in Table 1.

Table 1

	v. Kármán-Cochran results ($b \to \infty$)			Present results		
$z_1 = z/\delta$	F	G	$-H$	F	G	$-H$
0	0	1	0	0	1	0
0.5	0.154	0.708	0.092	0.154	0.708	0.092
1.	0.180	0.468	0.266	0.180	0.469	0.265
1.5	0.156	0.313	0.435	0.156	0.313	0.435
2	0.118	0.203	0.572	0.119	0.203	0.573
2.5	0.084	0.131	0.674	0.084	0.131	0.674
3	0.058	0.083	0.746	0.058	0.084	0.744
4	0.026	0.035	0.826	0.025	0.034	0.823

The agreement between the two sets of data is very good. Furthermore, v. Kármán-Cochran give $G'(0) = -0.616$ and $F'(0) = 0.510$, while we obtain $G'(0) = -0.6159$ and $F'(0) = 0.5101$.

It can be observed that F, G, and H have nearly reached their asymptotic behaviour already for $\delta = (1/8)\, z_F$.

The complete equivalence of system (2.19–21) in the limit $\delta \to 0$ to system (6.1–3) has been therefore assessed, and a successful check of our integration procedure has been performed.

§ 7. Comparison of the Numerical Results for the Viscous Torque with Experimental Data

The viscosity measurements are performed at constant effective driving torque τ_e by maintaining constant the excitation currents in the electromagnets. This is due to the difficulty of measuring the absolute values of τ_e. In such a way, τ_η turns out to be a constant, too. In this case, from (1.4) it follows

$$\eta \omega = A f(\delta), \quad (7.1)$$

where $A = (-\tau_\eta/\mu)$ is a constant. If we now suppose the edge effects to be negligible, (3.1) gives

$$\eta \omega = B g(\delta), \quad (7.2)$$

where $B = (-\tau_\eta z_F/\pi R_i^4)$ is a constant and $g(\delta) = \left(\dfrac{-\delta}{z_F G'(0)}\right)$.

However, if we have to take the edge effects into account, (3.6) gives

$$\eta \omega = C y(\delta), \quad (7.3)$$

where $C = -\tau_\eta z_F/[\pi R_i^4 (1 + k)]$ is a constant,

$$y(\delta) = \frac{(1 + k)\, g(\delta)}{1 + k\, g(\delta)}, \quad (7.4)$$

and $k = k_1 z_F$.

The experimental function $f(\delta)$ (7.1) has two important features: for small δ it increases linearly with δ and for large δ it saturates to the constant value 1. The functions $g(\delta)$ and $y(\delta)$ can be computed if $G'(0)$ is known as a function of the boundary layer thickness. In Fig. 6 such values are reported versus δ/z_F.

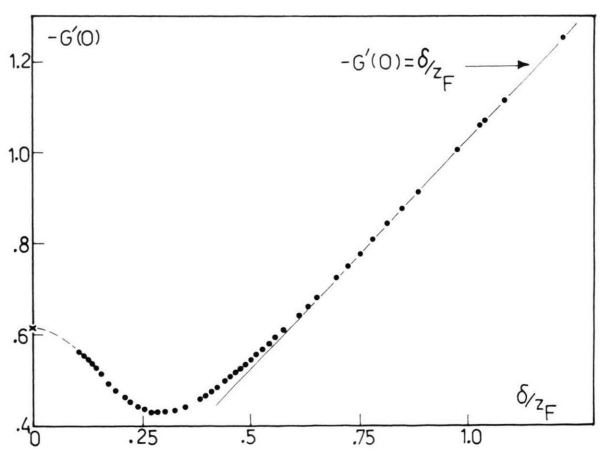

Fig. 6. Values of $-\dfrac{\mathrm{d}}{\mathrm{d}z_1} G(z_1)\Big|_{z_1=0} \equiv -G'(0)$ as functions of δ/z_F. For large δ/z_F, $-G'(0)$ is linear with δ. For small δ/z_F, it tends to the value $-G'(0) \simeq 0.616$ (indicated by symbol "x") of the disk immersed in an infinite medium. (Dashes show graphical extrapolation.)

For large δ/z_F, $G'(0)$ is given by

$$-G'(0) = \delta/z_F \tag{7.5}$$

so that $g(\delta) = 1$ and $y(\delta) = 1$. $-G'(0)$ goes through a minimum at $\delta/z_F \simeq 0.30$ and saturates to the constant value 0.616 for very small δ, so that in this region $g(\delta)$ is nearly proportional to δ. Therefore, as a matter of fact, $f(\delta)$ shares with $g(\delta)$ and $y(\delta)$ its limiting behaviour.

In Fig. 7 the experimental $f(\delta)$ and the theoretical functions $g(\delta)$ and $y(\delta)$ are plotted versus the bundary layer thickness. The values of $y(\delta)$ have been calculated by adjusting the value of the unknown constant k_1 until the minimum deviation from the experimental $f(\delta)$ occurred.

The function $g(\delta)$ is always lower than the experimental functions $f(\delta)$. This means that (3.1) is not correct for the disk in the housing for it neglects any edge effects. On the contrary, function $y(\delta)$ with $k \simeq 1.146$ does indeed approximate very well the experimental results to within a standard deviation of about 3×10^{-3}. This means that (3.6) accurately describes the torque on a rotating disk enclosed in a cavity. Furthermore, by comparing (1.4) with (7.1) and (7.3) and taking into account the explicit form of the coefficient C and that $f(\delta) \simeq y(\delta)$, we get

$$\mu = \frac{\pi R_i^4 (1+k)}{z_F}, \tag{7.5}$$

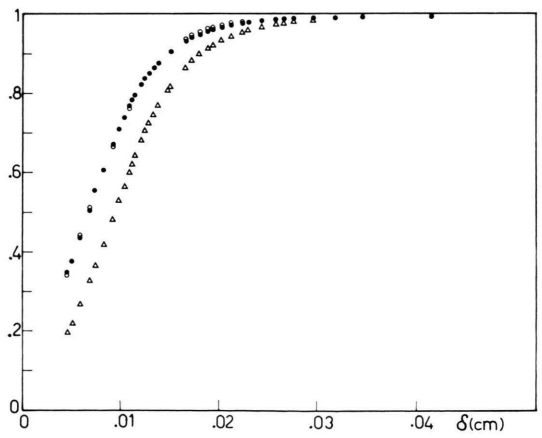

Fig. 7. In this figure the theoretical curves $y(\delta)$ (closed circles) and $g(\delta)$ (open triangles) are shown as functions of δ. Values of the experimental $f(\delta)$ are also plotted (open circles) where they significantly differ from $y(\delta)$.

and from (3.6) we get

$$\tau_\eta = \frac{-\pi R_i^4}{z_F} \eta \omega \frac{1 + k g(\delta)}{g(\delta)}. \tag{7.6}$$

We expect that edge effects are not very strong at small δ. In fact from (7.6), when $\delta \to 0$ $k g(\delta) \ll 1$ and can be neglected. Conversely, for large values of δ the edge effects grow very large and give a substantial contribution to the total torque. In our particular case, $k = 1.146$ and for $g(\delta) = 1$ the edge effects contribution to the torque amounts to about 53.4%. It is worth noting that the importance of this contribution can be varied by changing the geometrical dimension of the disk and of the cylindrical cavity as it can be seen by recalling (3.5), (3.3) and (3.4).

The experimental $f(\delta)$ has been interpolated with the following analytical form [1, 2]:

$$f(\delta) = (1 + \delta/\delta_0)\, d - \left\{2d - 1 + \left[1 - d\left(1 + \frac{\delta}{\delta_0}\right)\right]^2\right\}^{1/2}, \tag{7.7}$$

where

$$d = d_0 + d_1 [(\delta - \delta_0)^2 + d_2]^{-1} \tag{7.8}$$

and d_0, d_1, d_2 and δ_0 are fitting parameters whose determination was performed by calibration with N_2 at 30 °C in the pressure range 1 – 80 atm. The analytic form (7.7) of $f(\delta)$ reproduces the viscosity data of N_2 to within a standard deviation of about 0.075%.

We performed a non-linear least squares analysis [13] on $y(\delta)$, adopting the same analytical form of (7.7). In Table 2 the results of this analysis are compared with the experimental values of the fitting parameters:

Table 2

Experimental	Theoretical
$\delta_0 = 1.331 \times 10^{-2}$ (cm)	1.331×10^{-2}
$d_0 = 0.5046$	0.5046
$d_1 = 2.56 \times 10^{-7}$ (cm^2)	2.55×10^{-7}
$d_2 = 2.92 \times 10^{-5}$ (cm^2)	2.92×10^{-5}

The fitting parameters for both curves are identical. In such a way, (1.4) has been justified and, moreover, the functional form (7.7) of $f(\delta)$ has proven to be universal, because the fitting parameters are independent of the fluid used for the calibration of the apparatus. However, small differences exist between $f(\delta)$ and $y(\delta)$ (the largest diviation is about 0.8%) and these occur in an inter-

mediate range of δ: $0.016 \leq \delta \leq 0.021$ cm, corresponding to $2 \leq b \leq 2.6$.

In this range the total torque on the disk is not given by the simple superposition of the effects accounted for by (3.6), but it is a bit lower. In this region the contribution to the torque due to the radial gradient of the tangential velocity is overestimated ($\gamma(\delta) < f(\delta)$). To better determine the influence of the contribution due to the edge effects a more extensive experimentation on disks of different geometries is obviously required.

In Fig. 8 we have plotted the dimensionless torque coefficient

$$C_M = 2\,|\tau_\eta|\,/\varrho R_i^5 \omega^2 \tag{7.9}$$

as a function of the Reynolds number

$$R = (R_i/\delta)^2. \tag{7.10}$$

Our experimental data agree very well with our theoretical data as computed through (3.6). On the contrary, the C_M values computed through (3.1) are sensibly lower and tend to converge to the experimental ones as δ becomes small (large R), where the correction term k in (3.6) gives a smaller contribution.

For a large δ (small R) (3.6) gives

$$C_M \simeq \left(\frac{2\pi R_i}{z_F}\right)\frac{1+k}{R} \tag{7.11}$$

with $2\pi R_i (1+k)\, z_F^{-1} \simeq 293$ ($R_i = 0.9$ cm) as confirmed by the least squares analysis of the data for low R on both theoretical and experimental curves.

The presence of the lateral wall acts so as to increase the torque and hence the torque coefficient.

For fairly large R (small δ) C_M is nearly proportional to $R^{-1/2}$.

The case of the disk in an infinite fluid yields

$$C_M \simeq 3.87\, R^{-1/2}. \tag{7.12}$$

In our case, at $R \sim 3.83 \times 10^4$ (3.6) gives

$$C_M \simeq 4.33\, R^{-1/2}, \tag{7.13}$$

and then from the experimental curve we have

$$C_M \simeq 4.36\, R^{-1/2}. \tag{7.14}$$

Recalling that the disk in the infinite fluid is a particular case of our problem when $\delta \to 0\,(R \to \infty)$ it can be immediately recognized that the coefficients of (7.13–14) are already close to the limiting value of 3.87.

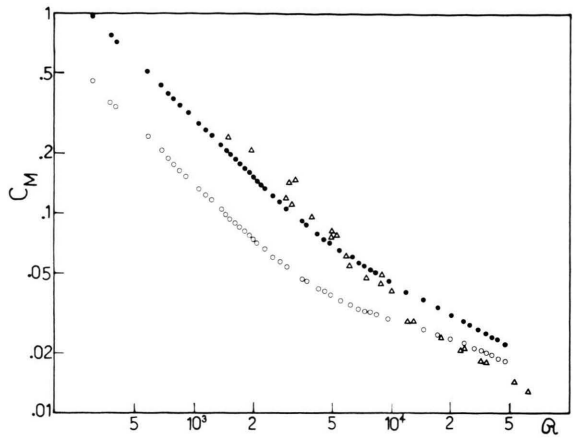

Fig. 8. Values of the dimensionless torque coefficient C_M versus the Reynolds number. Closed circles indicate both experimental results [1, 2] and the theoretical results obtained through (7.6) and (7.9). Open circles represent the theoretical results without taking into account any edge effects. Open triangles are results of other authors [12], drawn here for comparison.

For further comparisons, in Fig. 8 we have also plotted experimental results of other authors [12].

These results agree quite well with the present ones, even if they are much more scattered. The C_M values are larger because of different values of the geometrical constants of the devices ($z_F/R_i \simeq 0.02$ against $z_F/R_i \simeq 0.05$ in our case), but they also show a region where $C_M \propto R^{-1}$, and another where $C_M \propto R^{-1/2}$.

Furthermore, the transition from the R^{-1}- to the $R^{-1/2}$-behaviour takes place in about the same region as in our case.

§ 8. Conclusions

The direct numerical integration of the Navier-Stokes equations for the fluid motion induced by a rotating disk enclosed in a cylindrical cavity has given interesting results regarding two different problems.

The first, more theoretical one, is the determination of the components of the fluid velocity when the disk has an infinite radius. This helps determining the streamlines of the fluid. The velocity components we have found depend on the vertical height, z, above the disk in such a way to satisfy our physical intuition of the problem: at a given distance, r, from the center of the disk, the tangential

velocity monotonically decreases from the maximum value, ωr, on the disk to the minimum, zero, at the housing wall; the radial velocity changes sign to satisfy the continuity equation, while the axial velocity attains a maximum at a given height and is independent on r.

Unless the boundary layer thickness δ is not much larger than the gap z_F separating disk and housing wall, the z-dependent parts of the velocity components are not symmetric about the plane $z = z_F/2$. In this case, however, the radial and axial velocity components are practically zero, and the tangential velocity goes to zero linearly with $(z_F - z)$. This does indeed characterize the flow regime known as Couette-type flow.

As the boundary layer thickness decreases the asymmetry of the velocity components becomes more pronounced: a blurred secondary boundary layer is formed on the housing wall and there the flow is radially inwards. As δ further decreases, the equations for the disk in the housing tend to those for the disk immersed in an infinite fluid.

The second problem is concerned with the calculation of the retarding torque due to the fluid on a disk of finite radius in presence of a lateral wall. In this case, the lateral wall of the cylindrical housing drastically affects the fluid velocity field. In particular, the tangential velocity is not simply linearly dependent on the radius and this gives an additional contribution to the torque acting on actual disks which are cylinders of small, but finite height. This more realistic situation becomes evident when the computed torque acting on the disk is compared to experimental data. In fact, the torque calculated by neglecting such edge effects is lower than the measured one. On the contrary, on accounting for them, the theoretical curve agrees very well with the experimental one. We believe that the week disagreement ($< 1\%$) between the two curves is to be ascribed to the crude way of accounting for the edge corrections.

In any case, it has been demonstrated that the theoretically derived function (with edge effects corrections) can be expressed by an analytical form which is identical to that used for the experimental function. So it has also been proved that the results of the viscosity measurements obtained with the rotating disk viscometer do not depend upon the fluid used for calibrating the device.

Acknowledgements

The authors wish to thank Mr. C. Carraro and Dr. G. Torzo for many stimulating discussions.

[1] L. Bruschi and G. Torzo, Phys. Lett. **98A** (5–6), 265 (1983).
[2] L. Bruschi, M. Santini, and G. Torzo, J. Phys. E **17,** 312 (1984).
[3] M. Schlichting: "Boundary Layer Theory", McGraw-Hill, New York 1968, p. 97 and 609.
[4] L. Landau and E. Lifšits, Mècanique des fluids, MIR, Moscow 1971, Chapt. 5.
[5] M. H. Rogers and G. N. Lance, J. Fluid Mech. **7,** 617 (1959).
[6] Th. von Kármán, Z. Angew. Math. Mech. **1,** 233 (1921).
[7] W. G. Cochran, Proc. Cambridge Phyl. Soc. **30,** 365 (1934).
[8] K. Stewartson, Proc. Cambridge Phyl. Soc. **49,** 333 (1953).
[9] G. K. Batchelor, Quart. J. Mech. Appl. Math. **4,** 29 (1951).
[10] J. G. Dash and R. D. Taylor, Phys. Rev. **105** (1), 7 (1957).
[11] S. Albertoni, Appunti di calcolo numerico, Milan 1972, p. 115–124.
[12] F. Schultz-Grunow, Z. Angew. Math. Mech. **15,** 191 (1935).
[13] Ph. R. Bevington, Data Reduction and Error Analysis for the Physical Sciences. McGraw-Hill, New York 1969.